# Mg-MOF-74@SBA-15 hybrids: Synthesis, characterization, and adsorption properties

Anindita Chakraborty and Tapas Kumar Maji[a]
*Molecular Materials Laboratory, Chemistry and Physics of Materials Unit, Jawaharlal Nehru Centre for Advanced Scientific Research, Jakkur, Bangalore 560064, India*

(Received 15 September 2014; accepted 14 November 2014; published online 9 December 2014)

Nanocrystals of Mg-MOF-74 have been immobilized into the mesopores of SBA-15 rods to fabricate Mg-MOF-74@SBA-15 hybrid materials. To furnish such composites, a relatively simple synthetic strategy has been adopted by direct dispersion of the metal-organic framework (MOF) precursors in SBA-15 matrix to prepare the hybrid materials *in situ*. The hybrid materials have been characterized using powder X-ray diffraction and several spectroscopic and microscopic techniques, which suggest growth of the MOF nanocrystals inside the SBA-15 mesopores and the composites exhibit characteristics of both the components. $N_2$ adsorption isotherms at 77 K reveal that the composites contain additional mesopores, compared to only micropores of pristine MOF nanocrystals. In addition to such combination of both micro and mesoporosity, the composites also demonstrate significant $CO_2$ adsorption at room temperature.  [http://dx.doi.org/10.1063/1.4902816]

Porous coordination polymers (PCPs) or metal-organic frameworks (MOFs) are contemporary promising materials, which are uniformly ordered crystalline compounds that already have shown significant applications in various fields.[1–3] However, developing new hybrid systems has always fascinated materials scientists as such materials would bring interesting properties. A recent trend is to furnish functional composite of the MOFs or coordination compounds by hybridizing them with different active species like metal nanoparticles, oxides, quantum dots (QDs), polyoxometalates (POMs), polymers, graphene and graphene oxide (GO), carbon nanotubes (CNTs), boron nitride (BN), biomolecules, and mesoporous silica.[4–7] Such MOF composite materials can show unique properties and can serve as better materials than the individual components. We have recently shown that hybrid nanocomposites of ZIF-8 with GO exhibit high $CO_2$ storage capability and can also be used as the precursor for preparation of GO@ZnS nanocomposites.[7(a)] We have also shown that novel nanocomposites of MOF with BN nanosheet can demonstrate enhanced mechanical integrity preserving the functionality and microporosity of MOF.[7(b)]

The ordered mesoporous silica is a group of porous siliceous materials that have received considerable research interest due to their large surface areas and ordered porous structures.[8–10] They contain ordered pores with various pore symmetries (e.g., hexagonal, cubic, and lamellar) and can serve as an excellent support for dispersing a variety of guests like metal and oxide nanoparticles, enzymes, peptide and drug macromolecules.[11–13,21] Combination of mesoporous hard silica materials and the microporous crystalline MOF can be promising in various aspects like enhanced mechanical, chemical stability, novel gas adsorption behaviour, and as a stationary phase in liquid chromatography.[14–17] Li and Zeng have prepared hard core-shell MOF-mesoporous silica composite, that has shown improved mechanical stability than the parent soft MOFs.[14] Wang and co-workers have demonstrated that incorporation of MOF-5 into silica matrix improves the hydrostability of the MOF particles. High ammonia uptake by mesoporous silicate-MOF composites has also been realized.[15] However, MOF composites with mesoporous silica have not been explored

[a]E-mail: tmaji@jncasr.ac.in. Telephone: +91 80 2208 2826. FAX: +91 80 2208 2766.

 

adequately and most of the literature reports documenting fabrication of such composites require pre-functionalization of the silica substrate, thus making the synthesis complicated and tedious.[16] We conjecture that taking advantage of the mesopores of silicate materials, MOF particles can ideally be immobilized into the silicates and the resulting composite would exhibit characteristics of both the components.[17(a)]

Among the ordered mesoporous silicates, SBA-15 has been extensively studied which contains hexagonal 2D structure and facile synthetic route to prepare monodispersed SBA-15 rods has been documented.[9] We have prepared nanocrystals of Mg-MOF-74 *in situ* inside the mesopores of SBA-15 silica rods. MOF-74, also known as CPO-27-Zn, was first reported by Yaghi *et al.* and is a prototype MOF assembled from 2,5-dihydroxy-1,4-benzenedicarboxylate (DOBDC) linker and Zn(II) ions.[18] The Zn(II) ions produce linear, infinite-rod secondary building units (SBUs) bound by DOBDC resulting in a hexagonal, 1D pore structure (Scheme 1). The pores of the as-synthesized materials are filled with solvent molecules, which complete the coordination sphere of the metal ions. Upon desolvation, coordinatively unsaturated metal sites are generated which ensue significant $CO_2$ adsorption. The isostructural Mg(II) MOF was reported by Matzger and co-workers, which has shown the highest $CO_2$ adsorption at room temperature till date.[19] Combination of Mg-MOF-74 with SBA-15 is expected to fabricate a hybrid material that would show significant $CO_2$ adsorption at ambient condition along with typical mesoporous behaviour and we aimed to furnish such novel hybrids. We have avoided any complicated pre-functionalization of SBA-15 substrate and instead adopted a simple strategy to disperse the MOF crystals inside the mesopores of SBA-15, to produce the composite material *in situ*. We have grown nanocrystals of Mg-MOF-74 inside the mesopores of SBA-15 rods and the nanocrystals are expected to diffuse easily compared to the bulk MOF. Herein, we report synthesis, characterization, and adsorption study of hybrid Mg-MOF-74@SBA-15 materials with different amounts of loading of MOF nanocrystals into the SBA-15 matrix.

*Synthesis of SBA-15 rods*. Monodispersed SBA-15 was prepared following typical reaction conditions by Sayari and co-workers.[9] 4.0 g of triblock copolymer Pluronic P123 was added to a mixture of 30 ml of water and 120 g of 2 M HCl aqueous solution, which was stirred at 35 °C for overnight. 8.50 g of TEOS was then added to the solution under vigorous stirring. After 5 min of

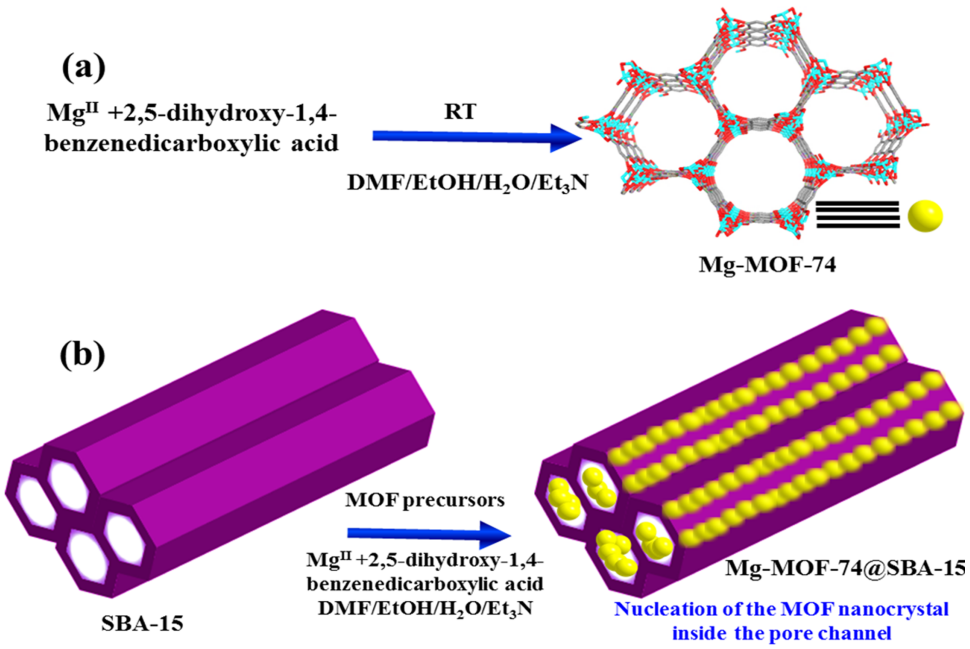


SCHEME 1. (a) Formation of Mg-MOF-74 nanocrystal at RT. The 3D framework along crystallographic *c* direction has been shown. Color code: Mg: cyan; C: grey; O: red. The yellow sphere corresponds to Mg-MOF-74 in nano phase. (b) A plausible mechanism of the growth of MOF nanocrystals inside the mesopores of SBA-15 resulting the Mg-MOF-74@SBA-15 composite.

stirring, the mixture was kept under static conditions at 35 °C for 20 h, followed by 24 h at 60 °C. The solid products were collected by filtration, washed with water, dried, and calcined at 550 °C in flowing air.

*Synthesis of Mg-MOF-74 nanocrystals*. Synthesis of well-defined Mg-MOF-74 nanocrystals of diameter ~100 nm was carried out at room temperature.[20] $Mg(NO_3)_2 \cdot 6H_2O$ (0.61 mmol) and 2,5-dihydroxy-1,4-benzenedicarboxylic acid (0.19 mmol) were dissolved in 15 ml of dimethyformamide (DMF). To this solution, a mixture of ethanol/water/triethylamine (1, 1, and 0.33 ml, respectively) was added under vigorous stirring and then the mixture was stirred for additional 2 h at room temperature. After the synthesis, the product was collected by centrifugation and was redispersed in fresh DMF. The suspension was heated at 100 °C for 2 h to dissolve other non-crystalline impurities.

*Synthesis of Mg-MOF74@SBA-15 composites*. Two different composites were prepared taking different amounts of calcined SBA-15. First, 60 mg of SBA-15 was taken in 15 ml of dimethyformamide and the solution was sonicated for 10 min. $Mg(NO_3)_2 \cdot 6H_2O$ (0.61 mmol) and 2,5-dihydroxy-1,4-benzenedicarboxylic acid (0.19 mmol) were then dissolved in the above solution. To this solution, a mixture of ethanol/water/triethylamine (1, 1, and 0.33 ml, respectively) was added under vigorous stirring and the mixture was stirred for additional 2 h at room temperature. The product Mg-MOF74@SBA-15 (**1**) was collected by centrifugation and was redispersed in fresh DMF. The suspension was heated at 100 °C for 2 h to dissolve other non-crystalline impurities. For synthesis of the second composite Mg-MOF74@SBA-15 (**2**), similar synthetic process was adopted except the fact that amount of SBA-15 used was 90 mg.

Powder X-ray diffraction (PXRD) patterns were recorded on a Bruker D8 Discover instrument using Cu–Kα radiation. Thermogravimetric analyses (TGA) were carried out on METTLER TOLEDO TGA850 instrument in the temperature range of 25–600 °C under nitrogen atmosphere (flow rate of 50 ml $min^{-1}$) at a heating rate of 5 °C $min^{-1}$. IR spectra were recorded on a Bruker IFS 66v/S spectrophotometer using KBr pellets in the region 4000–400 $cm^{-1}$. The morphologies of the composites were characterized with Transmission electron microscopy (TEM) (JEOL JEM-3010 with an accelerating voltage at 300 KV). Adsorption isotherms of $CO_2$ at 293 K and $N_2$ at 77 K were recorded with the dehydrated samples using QUANTACHROME QUADRASORB-SI analyser. The samples were subjected to solvent exchange with MeOH for 2 days prior to the activation. To prepare the dehydrated samples of nano Mg-MOF-74, SBA-15, and the composites **1** and **2**, approximately 70 mg of sample was taken in a sample holder and degassed at 180 °C under $10^{-1}$ pa vacuum for about 24 h prior to the measurements. Dead volume of the sample cell was measured using helium gas of 99.999% purity. The amount of gas adsorbed was calculated from the pressure difference ($P_{cal} - P_e$), where $P_{cal}$ is the calculated pressure with no gas adsorption and $P_e$ is the observed equilibrium pressure. All operations were computer-controlled and automatic.

The composites were characterized thoroughly. Figure 1 shows the PXRD patterns of Mg-MOF74@SBA-15 (**1**) and the simulated pattern of Mg-MOF 74. The well-correspondence between the two plots suggests formation of the crystalline phase of Mg-MOF-74 in the composite. Furthermore, the low angle peak in the composite (Figure 1 inset) similar to SBA-15 suggests presence of ordered mesopores corresponding to the SBA-15 constituent. The IR spectra of SBA-15, Mg-MOF-74, and the composites (**1** and **2**) were recorded and are given in Figure S1 in the supplementary material.[23] All vibrational bands assigned to Mg-MOF-74 are observed in **1** and **2**, which suggests that the composites contain Mg-MOF-74 phase. For SBA-15, an intense band is observed at 1083 $cm^{-1}$ due to the asymmetric vibration of Si-O-Si group. The characteristic bending vibration of Si-O-Si and the defective Si-O-H vibration were noted at 463 $cm^{-1}$ and 962 $cm^{-1}$, respectively. Similar bands were also observed for **1** and **2**, suggesting presence of SBA-15 phase in the composites. Figure S2 in the supplementary material represents the TGA profiles for as-syntheiszed MOF-74 nanocrystals, **1** and **2**.[23] The loading of the Mg-MOF-74 in the Mg-MOF-74@SBA-15 hybrids was estimated from the TGA measurements, based on the ratio of the weight loss of dried Mg-MOF-74@SBA-15 composite to the weight loss of the dried Mg-MOF-74 at ~250 °C, since SBA-15 does not show any weight loss at this temperature range.[9,17] The weight loss of dried Mg-MOF-74 is 32% at ~250 °C, while the loss for **1** and **2** at same temperature is 24% and 16%,

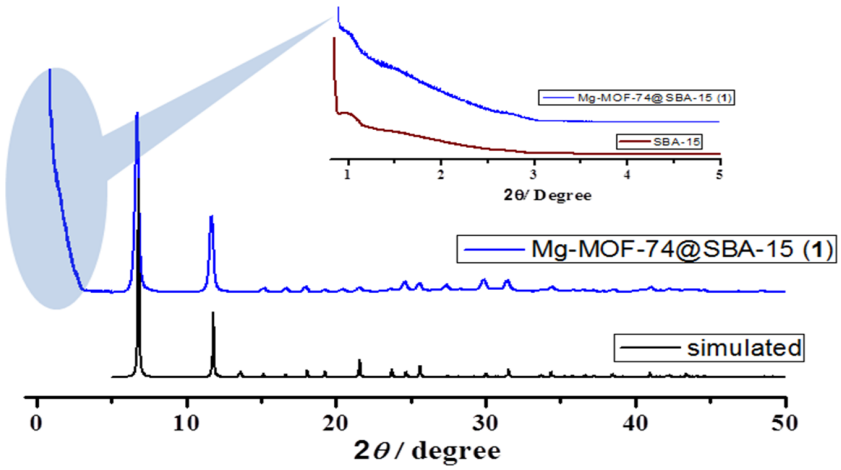


FIG. 1. The PXRD patterns of **1** and simulated pattern of Mg-MOf-74. The inset shows the low angle peak (similar to the SBA-15) of the composite suggesting presence of ordered mesopores.

respectively. Thus, the loading of Mg-MOF-74 in dried Mg-MOF-74@SBA-15 hybrid materials is estimated to be 75 wt. % (24/32) and 50 wt. % (16/32), for **1** and **2**, respectively.

To study the morphologies, SEM and TEM analyses of the compounds were carried out. We have recorded the SEM image of as-prepared SBA-15 particles, which shows SBA-15 rods with hexagonal face (Figure S3 in the supplementary material[23]). Figure 2 presents the SEM images of the composites showing formation of hybrid material of similar size of the as-prepared SBA-15 particles, suggesting Mg-MOF-74 nanoparticles are probably encapsulated into the SBA-15 materials. Energy dispersive X-ray spectroscopy (EDAX) analyses (Figures S4 and S5 in the supplementary material[23]) of the composites show presence of both Mg and Si elements coming from the Mg-MOF-74 and SBA-15, respectively. Furthermore, the element mapping (Figures S4 and S5 in the supplementary material[23]) suggests formation of composites with homogeneous distribution of the different elements throughout the samples. To get a closer view, TEM images (Figure 3) of as-prepared SBA-15 and one of the composite (**1**) were recorded. Figures 3(a) and 3(b) show the periodic siliceous structure of SBA-15. For **1**, similar siliceous structure is observed where most of the mesopores are occupied (as evident from the contrast) and few MOF crystals are also observed outside of the SBA-15 particles examined. Most of the MOF crystals are present inside the mesopores of SBA-15, suggesting that the nucleation of the nanocrystals of MOFs preferably occurs inside the channels of SBA-15, although the distribution is not completely even. Scheme 1 presents a schematic representation of a plausible mechanism of the growth of MOF nanocrystals

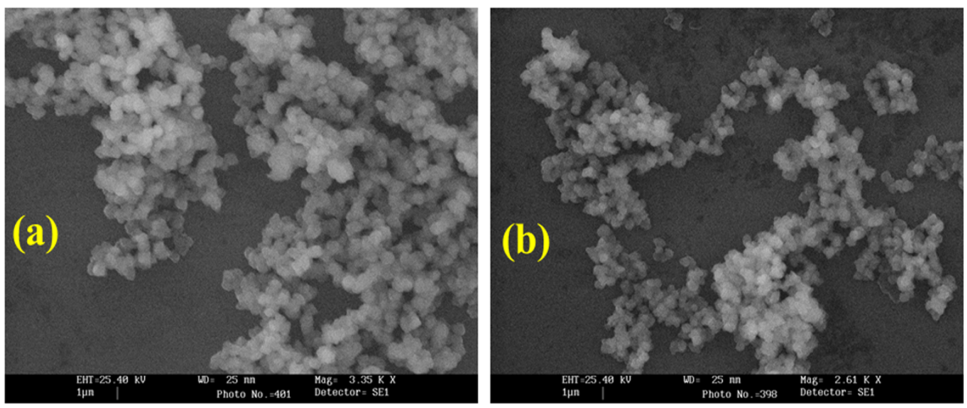


FIG. 2. SEM images of the (a) **1** and (b) **2**.

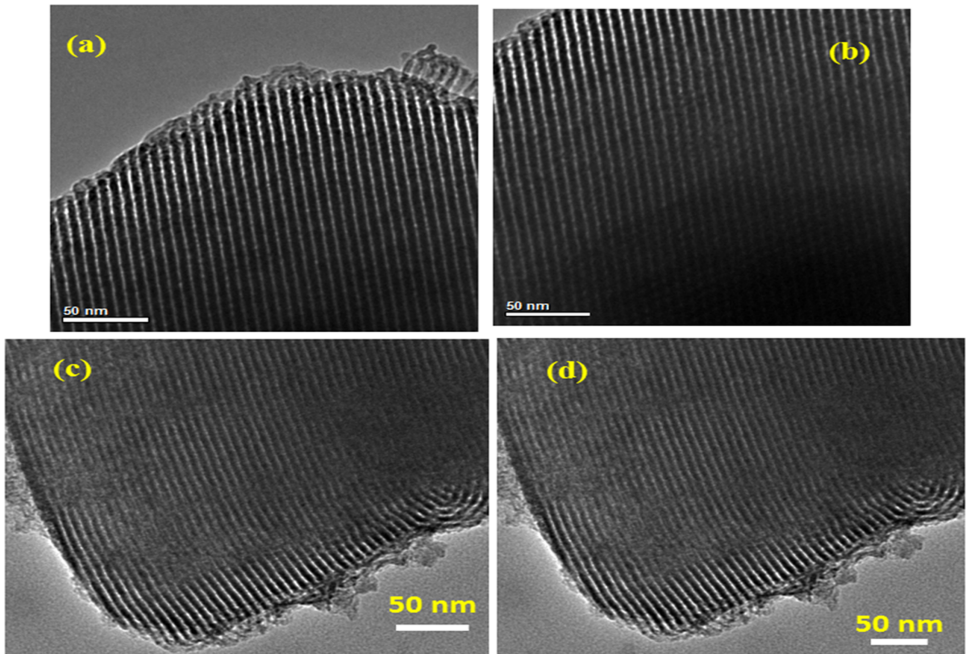


FIG. 3. (a) and (b) TEM images of as-prepared SBA-15. (c) and (d) TEM images of **1** showing that the periodic siliceous pores of SBA-15 are occupied by the MOF crystals. Few MOF crystals are observed outside the SBA-15 matrix.

inside the mesopores of SBA-15 resulting the Mg-MOF-74@SBA-15 composite. In the first step, the precursors of Mg-MOF-74 are added to SBA-15 matrix. In the next step, the nucleation of MOF nanocrystals starts and the nucleation should ideally be more favourable inside the mesopores rather than outside of SBA-15 since the internal surface can act as nanoreactors having greater affinity (due to the presence of silanol groups) for guest molecules.[17(a)] The periodically arranged pores having large pore volumes also facilitate rapid diffusion of MOF precursors from the solution to the pores, thus driving formation of most of the nanocrystals inside the pore. Thus, our synthetic strategy relies on simple and facile diffusion of the MOF nanocrystals into the mesopores.

To study the porosity of the desolvated hybrids, pristine Mg-MOF-74 and SBA-15, $N_2$ adsorption isotherms were measured using the activated samples at 77 K (Figure 4(a)). As reported, the isotherm of Mg-MOF-74 nanocrystals exhibits typical type I sorption behaviour due to the microporous nature with an uptake of 560 ml/g at $P/P_0 = 1$. The SBA-15 sample shows type IV adsorption isotherm, a typical characteristic of the mesopores. Interestingly, both desolvated composites (**1′** and **2′**) show a combination of type I (characteristic of microporous materials) and type IV (characteristic of mesoporous materials) profile. Thus the composites demonstrate presence of additional mesopores, compared to the only micropores of pristine MOF nanocrystals. At low $P/P_0$, it has the distinctive shape of a type I isotherm due to the micropore filing. Beyond $P/P_0 = 0.4$, the enhanced adsorption uptake up to the saturation point corresponds to multilayer formation and capillary condensation in bigger mesopores. The pore size distributions (using Barrett–Joyner–Halenda method) of SBA-15, **1′**, and **2′** are shown in Figure 4(b). It shows presence of mesopores (maximum distribution at ~32 Å) in the composites, similar to the SBA-15 rods. Since the MOF nanocrystals contain only micropores (pore size: $10.3 \times 5.5$ Å$^2$ (Ref. 18)), the mesopores in the composites originate from SBA-15. The decrease in pore sizes as well as adsorption uptake of the composites suggests partial filling of the mesopores by the MOF nanocrystals. This observation suggests growth of the MOF nanocrystals inside the mesopores rather than outside. Although the TEM images (Figure 3) show few MOF nanocrystals to be present outside the SBA matrix, the decrease in adsorption uptake and the partial filling of the mesopores of SBA confirmed that SBA-15 can potentially act as a microreactor for growth of MOF nanoparticles and most of the MOF nanoparticles must be present inside the SBA-15 channel. On the other hand, the micropore

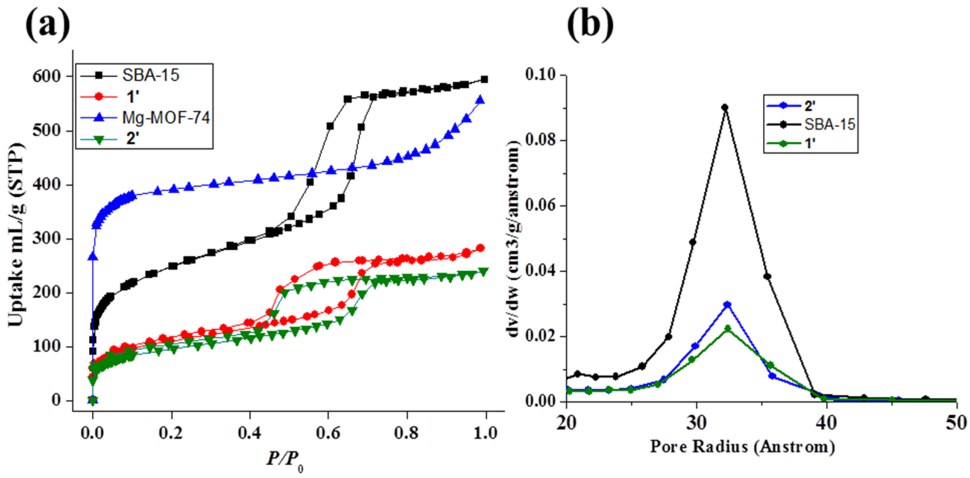


FIG. 4. (a) $N_2$ adsorption isotherms of Mg-MOF-74, SBA-15, **1′**, and **2′** at 77 K. (b) Pore size distribution of SBA-15, **1′**, and **2′**.

size distribution plot shows that the composites contain micropores in the same region as that of Mg-MOF-74 (Figure S6 in the supplementary material[23]).

$CO_2$ adsorption isotherm of MOF nanocrystals and the desolvated composites (**1′** and **2′**) at 293 K are presented in Figure 5 and Figure S7 in the supplementary material, respectively. Although the adsorption uptake for both the composites decreases from that of MOF nanocrystals, they show significant uptake (at $P/P_0 = 1$, 88 ml/g and 64 ml/g for **1′** and **2′**, respectively). **1′** and **2′** show 45% and 77% decrease in total uptake with respect to pristine MOF, respectively. The smaller $CO_2$ uptake by the composites compared to the pristine Mg-MOF-74 is probably due to the presence of SBA-15, which merely adsorbs any $CO_2$ at 293 K. Furthermore, for both composites, we observed hysteretic adsorption profile with smaller uptake at low pressure compared to pristine Mg-MOF-74. This can be explained based on confinement effect of Mg-MOF-74 inside the mesopores of SBA-15 resulting in a diffusion barrier in the adsorption and desorption paths for $CO_2$ molecules in the composites compared with that of pristine Mg-MOF-74. The hysteric profile of the composites indeed indicates kinetic trapping of $CO_2$ molecules in the hybrids. The profiles were also analyzed by the Dubinin–Radushkevich equation[22] to realize the adsorbate–adsorbent interaction, and the $q_{st,\phi}$ values for **1′** and **2′** are found to be ~30.3 and ~29.7 kJ $mol^{-1}$, respectively, suggesting strong interaction of $CO_2$ with the frameworks. Since SBA-15 is unable to provide strong interaction

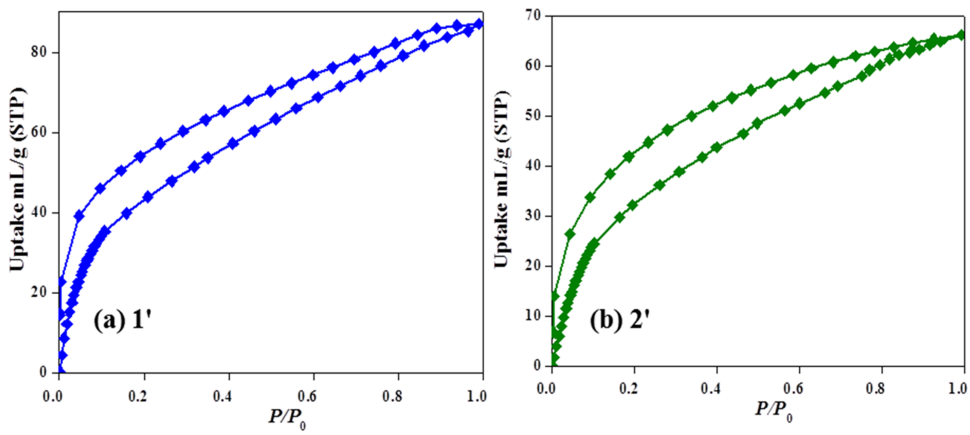


FIG. 5. $CO_2$ adsorption isotherms at 293 K of the desolvated composites (a) Mg-MOF-74@SBA-15 (**1′**) and (b) Mg-MOF-74@SBA-15 (**2′**).

sites (unsaturated $Mg^{II}$ sites in Mg-MOF-74) towards $CO_2$ molecules as Mg-MOF-74, the presence of SBA-15 components in the composites results decreased $CO_2$ uptake compared to pristine Mg-MOF-74. However, the mesoporous nature (as established from the $N_2$ physisorption measurements) of the composites along with such significant $CO_2$ adsorption capacity at room temperature makes the composites interesting porous materials.

Our work shows that by adopting a simple synthetic strategy by dispersing MOF precursors into the mesopores of SBA-15 rods, it is indeed possible to prepare novel MOF@SBA-15 hybrid materials *in situ*. SBA-15 can act as a nanoreactor for facile growth of the MOF nanocrystals and the composite material would thus exhibit characteristics of both the components (MOF and SBA-15). We have developed MOF@SBA-15 hybrid materials that show interesting adsorption behavior showing presence of both micro and mesopores. Such novel composite materials would open up new directions in materials science because hybridization of different interesting active components would result further new properties and phenomena.

[1] H.-C. Zhou, J. R. Long, and O. M. Yaghi, "Themed issue: Metal-organic frameworks," Chem. Rev. **112**, 673 (2012).
[2] S. Roy, A. Chakraborty, and T. K. Maji, Coord. Chem. Rev. **273–274**, 139 (2014).
[3] A. Chakraborty, R. Haldar, and T. K. Maji, Cryst. Growth Des. **13**, 4968 (2013).
[4] Q.-L. Zhu and Q. Xu, Chem. Soc. Rev. **43**, 5468 (2014).
[5] R. Kumar, K. Jayaramulu, T. K. Maji, and C. N. R. Rao, Dalton Trans. **43**, 7383 (2014).
[6] S. Pal, D. Jagadeesan, K. L. Gurunatha, M. Eswaramoorthy, and T. K. Maji, J. Mater. Chem. **18**, 5448 (2008).
[7] (a) R. Kumar, K. Jayaramulu, T. K. Maji, and C. N. R. Rao, Chem. Commun. **49**, 4947 (2013); (b) R. Kumar, D. Raut, I. Ahmad, U. Ramamurty, T. K. Maji, and C. N. R. Rao, Mater. Horiz. **1**, 517 (2014).
[8] C. T. Kresge, M. E. Leonowicz, W. J. Roth, J. C. Vartuli, and J. S. Beck, Nature **359**, 710 (1992).
[9] A. Sayari, B.-H. Han, and Y. Yang, J. Am. Chem. Soc. **126**, 14348 (2004).
[10] S. S. Kim, W. Zhang, and T. J. Pinnavaia, Science **282**, 1302 (1992).
[11] C. Coll, L. Mondragón, R. Martínez-Máñez, F. Sancenón, M. D. Marcos, J. Soto, P. Amorós, and E. Pérez-Payá, Angew. Chem., Int. Ed. **50**, 2138 (2011).
[12] A. Schlossbauer, D. Schaffert, J. Kecht, E. Wagner, and T. J. Bein, J. Am. Chem. Soc. **130**, 12558 (2008).
[13] H. Qi, K. E. Shopsowitz, W. Y. Hamad, and M. J. MacLachlan, J. Am. Chem. Soc. **133**, 3728 (2011).
[14] Z. Li and H. C. Zeng, J. Am. Chem. Soc. **136**(15), 5631 (2014).
[15] A. M. B. Furtado, J. Liu, Y. Wang, and M. D. LeVan, J. Mater. Chem. **21**, 6698 (2011).
[16] D. Buso, K. M. Nairn, M. Gimona, A. J. Hill, and P. Falcaro, Chem. Mater. **23**, 929 (2011).
[17] (a) C.-M. Wu, M. Rathi, S. P. Ahrenkiel, R. T. Koodali, and Z. Wang, Chem. Commun. **49**, 1223 (2013); (b) A. Kondo, S. Takanashi, and K. Maeda, J. Colloid Interface Sci. **384**, 110 (2012); (c) R. Ameloot, A. Liekens, L. Alaerts, M. Maes, A. Galarneau, B. Coq, G. Desmet, B. F. Sels, J. F. M. Denayer, and D. E. D. Vos, Eur. J. Inorg. Chem. 3735 (2010); (d) A. Ahmed, M. Forster, R. Clowes, D. Bradshaw, P. Myers, and H. Zhang, J. Mater. Chem. A. **1**, 3276 (2013).
[18] N. L. Rosi, J. Kim, M. Eddaoudi, B. Chen, M. O'Keeffe, and O. M. Yaghi, J. Am. Chem. Soc. **127**, 1504 (2005).
[19] S. R. Caskey, A. G. Wong-Foy, and A. J. Matzger, J. Am. Chem. Soc. **130**, 10870 (2008).
[20] T.-H. Bae and J. R. Long, Energy Environ. Sci. **6**, 3565 (2013).
[21] J. Fan, J. Lei, L. M. Wang, C. Z. Yu, B. Tu, and D. Y. Zhao, Chem. Commun. 2140 (2003).
[22] A. Kapoor, J. A. Ritter, and R. T. Yang, Langmuir **5**, 1118 (1989).
[23] See supplementary material at http://dx.doi.org/10.1063/1.4902816 for infrared spectra of Mg-MOF-74, SBA-15 and the composites, TGA of Mg-MOF-74 and the composites, SEM images of SBA-15, elemental mapping, EDX spectra and micropore size distribution plots for the composites and $CO_2$ adsorption isotherm of Mg-MOF-74 at 293 K.